Chiral magnetic interlayer coupling in synthetic antiferromagnets

Citation for published version (APA):
Han, D.-S., Lee, K., Hanke, J.-P., Mokrousov, Y., Yoo, W., Kim, T.-W., Lavijsen, R., You, C.-Y., Swagten, H. J. M., Jung, M.-H., & Klaeui, M. (2018). Chiral magnetic interlayer coupling in synthetic antiferromagnets. *arXiv*, *2018*(1809.01080), Article 1809.01080. https://doi.org/10.48550/arXiv.1809.01080

DOI:
10.48550/arXiv.1809.01080

Document status and date:
Published: 04/09/2018

Document Version:
Publisher's PDF, also known as Version of Record (includes final page, issue and volume numbers)

Chiral magnetic interlayer coupling in synthetic antiferromagnets

Dong-Soo Han[1,2†], Kyujoon Lee[1†], Jan-Philipp Hanke[1,3], Yuriy Mokrousov[1,3], Woosuk Yoo[4], Tae-Wan Kim[5], Reinoud Lavijsen[2], Chun-Yeol You[6], Henk J. M. Swagten[2], Myung-Hwa Jung[4*], and Mathias Kläui[1*]

1. Institute of Physics, Johannes Gutenberg-Universität Mainz, 55099, Mainz, Germany

2. Department of Applied Physics, Center for NanoMaterials, Eindhoven University of Technology, PO Box 513, 5600 MB Eindhoven, The Netherlands.

3. Peter Grünberg Institut and Institute for Advanced Simulation, Forschungszentrum Jülich and JARA, 52425 Jülich, Germany

4. Department of Physics, Sogang University, Seoul, Republic of Korea.

5. Department of Advanced Materials Engineering, Sejong University, Seoul, Republic of Korea

6. Department of Emerging Materials Science, DGIST, Daegu 42988, Republic of Korea

The exchange coupling underlies ferroic magnetic coupling and is thus the key element that governs statics and dynamics of magnetic systems. This fundamental interaction comes in two flavors - symmetric and antisymmetric coupling. While symmetric coupling leads to ferro- and antiferromagnetism, antisymmetric coupling has attracted significant interest owing to its major role in promoting topologically non-trivial spin textures[1–8] **that promise high-speed and energy-efficient devices.**[1,9–11] **So far, the antisymmetric exchange coupling rather short–ranged and limited to a single magnetic layer has been demonstrated**[1,12]**, while the symmetric coupling also leads to long-range interlayer exchange coupling. Here, we report the missing component of the long-range antisymmetric interlayer exchange coupling in perpendicularly magnetized synthetic antiferromagnets with parallel and antiparallel magnetization alignments. Asymmetric hysteresis loops under an in-plane field unambiguously reveal a unidirectional and chiral nature of this novel interaction, which cannot be accounted for by existing coupling mechanisms, resulting in canted magnetization alignments. This can be explained by spin-orbit coupling combined with reduced symmetry in multilayers. This new class of chiral interaction provides an additional degree of freedom for engineering magnetic structures and promises to enable a new class of three-dimensional topological structures.**[13,14]

† These authors contributed equally to this work.

* Authors to whom correspondence should be addressed: mhjung@sogang.ac.kr & klaeui@uni-mainz.de

Ferromagnets (FM) and antiferromagnets (AFM) possess collinear spin alignments within magnetic domains, due to a coupling, which is called *symmetric* or Heisenberg exchange coupling. While this conventional coupling is well known, recently a different coupling has moved into the forefront of interest, which leads to non-collinear and chiral spin textures. This new class of exchange coupling - *antisymmetric exchange coupling* ot Dzyaloshinskii-Moriya interaction (DMI)[15–17]– stems from the spin-orbit scattering of electrons, which mediate exchange coupling between neighboring spins within a FM, and an inversion asymmetry resulting in a finite amplitude of the net effect.[17–19] Therefore, DMI only manifests in systems with a spin-orbit coupling (SOC) and with a bulk or structural inversion asymmetry, e.g., in cubic B20 alloys or at interfaces between FMs and heavy metals (see Fig. 1a). In particular, the recent discovery of strong interfacial antisymmetric exchange coupling in perpendicularly magnetized multilayers– interfacial DMI - has stimulated work in the field of spintronics, opening fascinating new avenues for fundamental research[20] as well as highly efficient and fast spin-based information technologies.[1,9–11]

Besides the *intralayer* exchange coupling, in magnetic multilayers consisting of alternating ferromagnteic and non-magnetic spacer layers, the FMs can also be coupled to each other by *interlayer* exchange coupling (IEC).[14,21] Phenomenologically, the IEC shares common features with the symmetric Heisenberg exchange within each magnetic layer: they are bilinear in spins, and isotropic under rotation, favoring collinear spin alignment. In complete analogy to the experimentally established and theoretically understood symmetric and antisymmetric exchange within a single magnetic layer, one can anticipate that multilayers exhibit not only a symmetric but also an antisymmetric IEC. Specifically, based on simple symmetry considerations, it is natural to expect the emergence of such an antisymmetric IEC in systems with broken inversion symmetry (yellow and green boxes in Fig. 1b) and strong SOC provided by a non-magnetic spacer. A remarkable feature of the antisymmetric IEC is that it promotes chiral magnetization configurations perpendicular to the film plane, in contrast to the interfacial DMI leading to chiral spin structures within individual layers. This suggests the possibility for designing three-dimensional topological structures based on this novel interaction. Despite its fundamental importance as well as the associated technological promises, [10,14,22,23] clear evidence of the antisymmetric IEC is remarkably elusive so far. In this Letter, we present the experimental demonstration of such a hitherto uncovered antisymmetric IEC in perpendicularly magnetized synthetic antiferromagnets (SAFs) with parallel and antiparallel magnetization alignments. We study the multilayer reversal in different stacks and using judiciously designed field sequences, we can identify from unidirectional and chiral magnetization reversal the presence of an antisymmetric IEC.

We start by developing the necessary concepts to unambiguously identify the effect of antisymmetric IEC. In general, the magnetization reversal in FMs is invariant upon the inversion of the magnetic field direction. However, this field-reversal invariance does not hold if the inversion symmetry is broken in a given physical system. One particular example is the interfacial DMI.[17] In the presence of interfacial DMI, domain walls (DWs) experience different effective fields according to their magnetic orderings, up-to-down (U-D) and down-to-up (D-U), under an in-plane magnetic field H_{IN} as the core magnetizations within DWs of U-D and D-U align along opposite directions due to their preferred handedness by DMI. Consequently, when the DW moves, its velocity becomes asymmetric with respect to H_{IN}, depending on their magnetic ordering.[1,3,24,25]

Analogously, the antisymmetric IEC can break the field-reversal symmetry for the magnetization reversal. In the absence of the antisymmetric IEC, H_{IN} cannot break the inversion symmetry but only assist in lowering the energy barrier for the magnetization reversal independent of the switching polarity (left panels of Fig.1c and 1d). However, if the antisymmetric IEC is present, the chiral magnetization configurations are affected differently by H_{IN}, assisted or hindered in their magnetization switching depending on the sign of H_{IN} and the magnetization configurations. Particularly, they exhibit contrasting energy barriers for magnetization switching from parallel to antiparallel and antiparallel to parallel alignments as well as for switching of D-U and U-D, as shown in right panels of Fig. 1c and 1d. (Supplementary Note I) Accordingly, one would expect different switching fields with respect to the sweeping direction of the magnetic field, which in turn results in the asymmetric magnetic hysteresis loops.

To test experimentally if the aforementioned asymmetric switching exists, which would indicate the presence of antisymmetric IEC, we measure the switching fields of typical SAFs of Ta(4)/ Pt(4)/ Co(0.6)/ Pt(0.5)/ Ru(t_{Ru})/ Pt(0.5)/ Co(1)/ Pt(4) (layer thicknesses in nanometers), by sweeping the out-of-plane magnetic field, H_z, whilst simultaneously applying H_{IN} (Methods section). Here two Co layers are coupled to each other via the symmetric IEC and perpendicularly magnetized with either parallel or antiparallel magnetization alignments at its remanence. The magnetic hysteresis loops are measured by anomalous Hall effect (AHE), using the measurement configurations shown in Fig. 1e. For comparison, we also measure the switching fields of the reference sample Pt/Co/Pt/Ru that is nominally the same as the bottom half of the SAFs but without any IEC.

Figure 2a shows the magnetic hysteresis loops of Pt/Co/Pt/Ru and Pt/Co/Pt/Ru/Pt/Co/Pt where t_{Ru}=0.4 and 2.7 nm, for which the symmetric IEC is ferromagnetic and antiferromagnetic leading to parallel and antiparallel alignment of the layers, respectively. Square hysteresis loops are clearly seen for all structures, showing that they have strong perpendicular magnetization anisotropy (PMA). Importantly, we find that the hysteresis loops for the SAFs with parallel and antiparallel coupling become significantly asymmetric when H_{IN} is applied. For the parallel coupling case, at $|\mu_0 H_{IN}|$ = 100mT, a difference of approximately 0.7 mT in the switching fields ($\Delta\mu_0 H_{SW}$) between U-D and D-U is found. For the antiparallel coupling case, the hysteresis loop is seemingly biased to the left (right) at $\mu_0 H_{IN}$= 100mT (-100mT), giving rise to $\Delta\mu_0 H_{SW}$ = 1.1 and 1.4 mT for switching from parallel to antiparallel and from antiparallel to parallel alignments, respectively. Such asymmetric behavior is in striking contrast to the results obtained from our reference sample of Pt/Co/Pt/Ru, where the magnetic hysteresis loops are symmetric with respect to H_z=0 irrespectively of the sign of H_{IN}. The measured absence of inversion symmetry in the hysteresis loops is in obvious disagreement with the field-reversal symmetry, demonstrating the presence of a symmetry-breaking interaction such as antisymmetric IEC in our SAFs. Moreover, we note that the field-reversal symmetry for Pt/Co/Pt/Ru in the same setup also excludes any possible artifact from the misalignment of the in-plane magnet, which could otherwise cause an asymmetry in the hysteresis loop.

To understand the origin of the asymmetric switching behavior, we next measure the azimuthal-angular dependence of H_{SW}, as shown in Fig. 2b and 2c. Here, the magnitude of the in-plane field is kept at $|\mu_0 H_{IN}|$ = 100 mT, while rotated from 0° to 360°. In systems with inversion symmetry, one expects to see an isotropic or uniaxial (or multiaxial) anisotropy depending on the crystalline properties of thin films, which is indeed found in our reference sample (see Fig. 2b). Notably, however, we find that the magnetization switching for both SAFs with parallel and antiparallel alignment exhibits a unidirectional anisotropy which is for parallel (antiparallel) alignment with symmetric (**S**) and asymmetric (**AS**) along the direction of $\mathbf{H}_{IN}$ // 75° (150°) and $\mathbf{H}_{IN}$ // 165° (240°), respectively (this will be discussed in detail later). This highlights the *unidirectional* nature of the observed interlayer coupling. Interestingly, for the antiparallel coupling, we obtain markedly different unidirectional features in the two magnetic layers: for the case of the top Co layer (FM_{top}), the value of $|\mu_0 H_{SW}|$ for the U-D (D-U) is biased to 60° (240°), while for the bottom Co layer (FM_{bottom}), it is biased along the opposite direction. This opposite unidirectional behavior between two magnetic layers unambiguously reveals that the observed unidirectional effect has a chiral nature (see Supplementary Note 1) in line with an antisymmetric IEC. Here, we would like to note that the observed chiral behavior is radically different from that expected from currently known magnetic interactions. For example, the biquadratic IEC[26] can also introduce similar non-collinear configurations, leading, however, to isotropic behavior without preferred handedness, contrary to our observations as seen in Fig. 2c. Furthermore, the interfacial DMI cannot account for such asymmetric switching behavior, as this interaction cannot produce the obtained asymmetric hysteresis on its own unless it is combined with additional symmetry breaking effects such as DC spin currents[27] or laterally asymmetric nanostructures[28] (see Supplementary Note 2)

The antisymmetric IEC is expected in particular to modify the dependence of H_{SW} on H_{IN}, which we plot in Fig. 3. For the structure with parallel coupling, the asymmetric behavior between U-D and D-U switching is again clearly found for the case where the H_{IN} is applied along the **AS** axis, while almost symmetric behavior is seen for $\mathbf{H}_{IN}$ // **S**. (Fig. 3a and 3c) In particular, for the antiparallel coupling case, one can see that the $\mathbf{H}_{IN}$ for local maxima (or minima) are shifted away from H_{IN} =0 mT for $\mathbf{H}_{IN}$ // **AS**, and the direction of the shift reverses for the opposite switching polarity. (Fig. 3b) This shift of H_{SW} along the H_{IN} axis is a robust indicator for the presence of the antisymmetric IEC; the offset in curves of H_{SW} vs. H_{IN} indicates the presence of a built-in effective field, the sign and magnitude of which rely on the relative orientation of the magnetization between the top and bottom Co layers. This is analogous to the internal fields from the interfacial DMI, which depends on the magnetic ordering of DW structures.[24] However, this is in sharp contrast to the case without the antisymmetric IEC, where H_{IN} always assists in switching the magnetization of perpendicularly magnetized materials irrespectively of the sign of H_{IN} and switching polarity. To validate the found asymmetric switching behavior by the antisymmetric IEC, we perform numerical calculations based on a macro-spin model incorporating the symmetric and antisymmetric IEC (Methods section). The calculated azimuthal-angular and field-dependence of H_{SW} for the parallel and antiparallel couplings are presented in Fig. 3c and 3d. The numerical calculations are qualitatively in good agreement with the experimental data, clearly reproducing the asymmetric and off-centered H_{SW} vs. H_{IN} as well as the unidirectional and chiral azimuthal-angular dependence of H_{SW} (see Supplementary Note 3). This firmly supports our conclusion that the unidirectional switching behavior is attributed to the antisymmetric IEC. The quantitative values of switching fields and the switching sequences of top and bottom Co layers are found to be different from our numerical calculations. This is most likely due to the computational parameters chosen, thermal effects and dipolar interaction that are not taken into account in calculations but are present in the experiments.[29]

To put our experimental findings on solid theoretical foundations and uncover the minimal ingredients that give rise to the observed antisymmetric IEC, we employ theoretical *ab initio* methods to scrutinize this coupling in thin magnetic heterostructures (Methods section and Supplementary Note 4). In particular, we focus on the system Co/Ru/Pt/Co with collinear magnetization within each layer. To explore the effect of the in-plane symmetry in multilayers on the antisymmetric IEC, in our calculations, we consider various C_{1v} in-plane locations of the top Co between the hollow sites "a" and "b" of C_{3v} symmetry as illustrated in Fig. 4a. One of the key manifestations of the antisymmetric IEC $\mathbf{D}_{\mathrm{inter}} \cdot (\mathbf{S}_1 \times \mathbf{S}_2)$ is a relativistic contribution to the total energy that is asymmetric with respect to the relative angle α between the magnetic moments $\mathbf{S}_1$ and $\mathbf{S}_2$ in the two Co layers. Indeed, our electronic-structure calculations demonstrate such a unique signature of the antisymmetric IEC in the low-symmetric C_{1v} structures (see Fig. 4b and Fig. S6), generally favoring a non-zero canting between adjacent ferromagnetic layers due to the complex interplay with the conventional symmetric IEC. To assess the overall relevance of such a chiral interlayer interaction, we estimate for comparison the magnitude of the symmetric IEC $J_{\text{inter}}\left(\mathbf{S}_1 \cdot \mathbf{S}_2\right)$ by using an effective parameter J_{inter} that describes the small-angle region in the non-relativistic energy dispersion. Figure 4c presents the calculated values of both interlayer exchange interactions as a function of the position of the top magnet for an originally ferromagnetic or antiferromagnetic coupling between the magnetic layers. While the symmetric coupling exceeds the typical energy scale for the chiral IEC of 1.0 meV by one to two orders of magnitude in the studied system, the latter interaction is more susceptible to changes in the symmetry of the crystal lattice. In particular, the characteristic vector $\mathbf{D}_{\text{inter}}$ is required to be perpendicular to any mirror plane connecting interaction partners in the two layers, which renders the net antisymmetric IEC zero in C_{3v} systems but generally finite in the case of reduced symmetry (see Fig. 4b). By emphasizing the key role of the in-plane symmetry breaking for this novel magnetic interaction, we note that any effective symmetry breaking, e.g., from a thickness gradient or a lattice mismatch between different atomic layers leading to dislocations, can give rise to the appearance of the antisymmetric IEC. Indeed, we experimentally demonstrate that a small thickness gradient in our samples gives rise to an effective symmetry breaking, allowing the antisymmetric IEC with a fixed $\mathbf{D}_{\text{inter}}$ perpendicular to the thickness gradient direction (see Supplementary Note 5). Additionally, for an appropriately asymmetric system, our *ab initio* calculations clearly confirm the presence of the antisymmetric IEC, which predominantly acquires its microscopic contribution from the heavy metals like Pt, as a direct consequence of SOC. Therefore, we anticipate that the predicted effect of an antisymmetric IEC, as well as the corresponding chiral spin textures, can be designed by adjusting the interface chemistry,[17] or by tuning the thickness of the Ru spacer layer[30] to alter the coupling between adjacent magnetic layers.

Complementing the ensemble of magnetic interactions in systems with broken inversion symmetry, our combined experimental and theoretical work establishes the antisymmetric IEC of two adjacent magnetic layers mediated by a non-magnetic spacer as an integral part for understanding and controlling three-dimensional magnetic textures. Specifically, we experimentally demonstrate the existence of this novel IEC in SAFs with parallel and antiparallel alignments, leading to asymmetric switching behaviors under in-plane bias fields. The observed asymmetric magnetization reversal is a unique signature of the chiral magnetization in the interlayer exchange-coupled layers. We identify the interplay of SOC and the reduced symmetry as the microscopic origin of the observed antisymmetric IEC. Our findings not only uncover the hidden magnetic interaction in SAFs with parallel and antiparallel coupling but also open the possibility for three-dimensional topological structures.

Acknowledgments

We acknowledge insightful discussions with Markus Hoffmann, Stefan Blügel, Bertrand Dupé, and Kyoung-Whan Kim. D.-S. H, K.L, and M.K acknowledge support from MaHoJeRo (DAAD Spintronics network, project number 57334897) and the German Research Foundation (in particular SFB TRR 173 Spin+X). K.-J. L. acknowledges the European Union’s Horizon 2020 research and innovation programme under the Marie Skłodowska-Curie grant agreement Standard

EF No. 709151. C.-Y. You acknowledges support from the National Research Foundation of South Korea under Grant 2017R1A2B3002621, and DGIST Research and Development Program under Grant 18-BT-02. M.-H. J. acknowledges support from the National Research Foundation of Korea (NRF) grant funded by the Korea government (MEST) (No. 2017R1A2B3007918). J.-P. H. and Y. M. gratefully acknowledge computing time on the supercomputers JUQUEEN and JURECA at Jülich Super-computing Center, and at the JARA-HPC cluster of RWTH Aachen, as well as funding under SPP 2137 "Skyrmionics" (project MO 1731/7-1) and project MO 1731/5-1 of Deutsche Forschungsgemeinschaft (DFG). D.-S. H., H. J. M. S., and R. L acknowledge support from the research program of the Foundation for Fundamental Research on Matter (FOM), which is part of The Netherlands Organisation for Scientific Research (NWO).

Authors contribution

M.-H. J. and D.-S. H. conceived the original idea. D.-S. H. and K. L. planned and designed the experiments. D.-S. H. performed the sample fabrication with support from R. L. and H. J. M. S.. D.-S. H. and K. L. performed transport measurements with W. Y. and data analysis under the supervision of M. K. and M.-H. J.. J. P. H. and Y. M. performed the first-principle calculations and the analysis of relevant data. D.-S. H. and C.-Y. Y. performed the numerical calculation based on a macro-spin model. D.-S. H. wrote the paper with K. L., J. H., and M.K. All authors discussed the results and commented on the manuscript.

Methods

Sample preparation and anomalous Hall measurement.

The magnetic multilayers were grown on a silicon wafer coated with a 100nm-thick SiO_2 by using a UHV magnetron DC sputtering system at the base pressure of 9.5×10^{-8} mbar and the working pressure of 2×10^{-2}mbar. Multilayers of Si/Ta(4)/Pt/(4)/Co(1.0)/Pt(0.7)/Ru(t)/Pt(0.7)/Co(0.9)/Pt(4) were grown at room temperature (layer thicknesses in nm). The Ru is used for the spacer which provides strong IEC, and the Pt layers between top and bottom Co layers are used to enhance the PMA of both ferromagnetic layers. To investigate the Ru-thickness dependent interlayer coupling, a wedge-shaped sample of Ta/Pt/Co/Pt/Ru/Pt/Co/Pt, where the Ru thickness was varied from 0 to 4nm, was preliminarily grown, and the oscillatory behavior of magnetic hysteresis loops was measured by the magneto-optical Kerr effect in a polar configuration (pMOKE). The Ru thicknesses used in the main text and supplementary notes were selected from the result. The hysteresis loops of the magnetic multilayers were measured by anomalous Hall signal on approximately 5×5 mm^2 sized continuous film by using a Van der Pauw method. For the transport measurement, a sinusoidal current with a frequency of 13.7Hz and a peak-to-peak amplitude of ~1mA was used as a current source, Lock-in technique was used for detecting the Hall signal.

Macro-spin modeling.

In order to explore the effect of the antisymmetric IEC and other magnetic interactions on the magnetization reversal, we employed a macro-spin model that finds an equilibrium magnetization configuration through minimization of the total free energy functional which consists of anisotropic energy, Zeeman energy, symmetric and antisymmetric exchange energies, that is given by

$$\begin{aligned} E_{tot} = &-\mu_0 M_{S,\mathrm{top}} t_{\mathrm{top}} \mathbf{m}_{\mathrm{top}} \cdot \mathbf{B} - \mu_0 M_{S,\mathrm{bottom}} t_{\mathrm{bottom}} \mathbf{m}_{\mathrm{bottom}} \cdot \mathbf{B} - K_{\mathrm{top}} t_{\mathrm{top}} \left(\mathbf{m}_{\mathrm{top}} \cdot \hat{z}\right) - K_{\mathrm{bottom}} t_{\mathrm{bottom}} \left(\mathbf{m}_{\mathrm{bottom}} \cdot \hat{z}\right) \\ &- J_{\mathrm{inter}} \mathbf{m}_{\mathrm{top}} \cdot \mathbf{m}_{\mathrm{bottom}} - \mathbf{D}_{\mathrm{inter}} \cdot \left(\mathbf{m}_{\mathrm{top}} \times \mathbf{m}_{\mathrm{bottom}}\right) \end{aligned}$$

Here, M_s is saturation magnetization, $\mathbf{m}$ magnetization vector, K effective anisotropy constant, μ_0 vacuum permeability**,** $\mathbf{B}$ external magnetic field, t thickness of a magnetic layer, $\hat{z}$ unit vector normal to surface, J_{inter} coefficient for symmetric IEC, and D_{inter} DMI vector for antisymmetric IEC. The subscript of "top" and "bottom" describe the top and bottom magnetic layers, respectively. For a model system of Pt/Co/Pt/Ru/Pt/Co/Pt, we used the following material parameters: M_s= 1.1×10^6 A/m, K = 2.24×10^5 and 5.25×10^5 J/m^3 for the bottom and top layers, respectively. The coefficients for the symmetric IEC J_{inter} = 2.1×10^{-4} and -2.0×10^{-4} mJ/m^2 and the antisymmetric IEC, D_{inter} corresponding to $|D_{inter}/J_{inter}|$ = 0.1 and 0.03 were used for the SAFs with parallel and antiparallel coupling, respectively.

First-principles calculations.

Using material-specific density functional theory as implemented in the full-potential linearized augmented-plane-wave (FLAPW) code FLEUR,[31] we studied the electronic structure of a thin Co/Ru/Pt/Co film in a super-cell geometry. The lattice constant of the in-plane hexagonal lattice was 5.211 a_0 (where a_0 is Bohr's radius), the distance between the two Co layers was 12.765 a_0, and we assumed a face-centered cubic stacking but variable in-plane positions of the top magnetic layer. Based on the generalized gradient approximation,[32] the self-consistent calculations of the system without SOC were performed using a plane-wave cutoff of 4.0 a_0^{-1}, and the full Brillouin zone was sampled by 1024 points. By including the effect of SOC to first order, we unambiguously determined the magnitude of the antisymmetric interlayer exchange interaction from the change in the energy dispersion of coned spin spirals[33] propagating perpendicular to the film. In these force-theorem calculations with SOC, the Brillouin zone was sampled by 4096 points. Choosing a large enough distance between different super cells, we explicitly ensured that periodic images of the slab do not contribute to the obtained magnetic interaction parameters.

References

1. Emori, S., Bauer, U., Ahn, S.-M., Martinez, E. & Beach, G. S. D. Current-driven dynamics of chiral ferromagnetic domain walls. *Nat. Mater.* **12,** 611–616 (2013).

2. Miron, I. M. *et al.* Fast current-induced domain-wall motion controlled by the Rashba effect. *Nat. Mater.* **10,** 419–423 (2011).

3. Ryu, K.-S., Thomas, L., Yang, S.-H. & Parkin, S. Chiral spin torque at magnetic domain walls. *Nat. Nanotechnol.* **8,** 527–533 (2013).

4. Mühlbauer, S. *et al.* Skyrmion lattice in a chiral magnet. *Science (80-.).* **323,** 915 (2009).

5. Yu, X. Z. *et al.* Skyrmion flow near room temperature in an ultralow current density. *Nat. Commun.* **3,** 988 (2012).

6. Woo, S. *et al.* Observation of room-temperature magnetic skyrmions and their current-driven dynamics in ultrathin metallic ferromagnets. *Nat. Mater.* **15,** 501–506 (2016).

7. Litzius, K. *et al.* Skyrmion Hall effect revealed by direct time-resolved X-ray microscopy. *Nat. Phys.* **13,** 170–175 (2016).

8. Moreau-Luchaire, C. *et al.* Additive interfacial chiral interaction in multilayers for stabilization of small individual skyrmions at room temperature. *Nat. Nanotechnol.* **11,** 444–448 (2016).

9. Parkin, S. S. P., Hayashi, M. & Thomas, L. Magnetic Domain-Wall Racetrack Memory. *Science (80-.).* **320,** 190 (2008).

10. Yang, S.-H., Ryu, K.-S. & Parkin, S. Domain-wall velocities of up to 750 m s−1 driven by exchange-coupling torque in synthetic antiferromagnets. *Nat. Nanotechnol.* **10,** 221 (2015).

11. Kim, K.-J. *et al.* Fast domain wall motion in the vicinity of the angular momentum compensation temperature of ferrimagnets. *Nat. Mater.* **16,** 1187 (2017).

12. Bode, M. *et al.* Chiral magnetic order at surfaces driven by inversion asymmetry. *Nature* **447,** 190–193 (2007).

13. Fernández-Pacheco, A. *et al.* Three-dimensional nanomagnetism. *Nat. Commun.* **8,** 15756 (2017).

14. Lavrijsen, R. *et al.* Magnetic ratchet for three-dimensional spintronic memory and logic. *Nature* **493,** 647–650 (2013).

15. Dzyaloshinsky, I. A thermodynamic theory of "weak" ferromagnetism of antiferromagnetics. *J. Phys. Chem. Solids* **4,** 241–255 (1958).

16. Moriya, T. Anisotropic Superexchange Interaction and Weak Ferromagnetism. *Phys. Rev.* **120,** 91–98 (1960).

17. Fert, A. & Levy, P. M. Role of Anisotropic Exchange Interactions in Determining the Properties of Spin-Glasses. *Phys. Rev. Lett.* **44,** 1538–1541 (1980).

18. Kundu, A. & Zhang, S. Dzyaloshinskii-Moriya interaction mediated by spin-polarized band with Rashba spin-orbit coupling. *Phys. Rev. B* **92,** 94434 (2015).

19. Imamura, H., Bruno, P. & Utsumi, Y. Twisted exchange interaction between localized spins in presence of Rashba spin-orbit coupling. *AIP Conf. Proc.* **772,** 1409–1410 (2005).

20. Kim, S. *et al.* Correlation of the Dzyaloshinskii–Moriya interaction with Heisenberg exchange and orbital asphericity. *Nat. Commun.* **9,** 1648 (2018).

21. Grünberg, P., Schreiber, R., Pang, Y., Brodsky, M. B. & Sowers, H. Layered Magnetic Structures: Evidence for Antiferromagnetic Coupling of Fe Layers across Cr Interlayers. *Phys. Rev. Lett.* **57,** 2442–2445 (1986).

22. Duine, R. A., Lee, K.-J., Parkin, S. S. P. & Stiles, M. D. Synthetic antiferromagnetic spintronics. *Nat. Phys.* **14,** 217–219 (2018).

23. Yang, Q. *et al.* Ionic liquid gating control of RKKY interaction in FeCoB/Ru/FeCoB and (Pt/Co)2/Ru/(Co/Pt)2 multilayers. *Nat. Commun.* **9,** 991 (2018).

24. Je, S.-G. *et al.* Asymmetric magnetic domain-wall motion by the Dzyaloshinskii-Moriya interaction. *Phys. Rev. B* **88,** 214401 (2013).

25. Lo Conte, R. *et al.* Role of B diffusion in the interfacial Dzyaloshinskii-Moriya interaction in Ta/Co20Fe60B20/MgO nanowires. *Phys. Rev. B* **91,** 14433 (2015).

26. Demokritov, S. O. Biquadratic interlayer coupling in layered magnetic systems. *J. Phys. D. Appl. Phys.* **31,** 925 (1998).

27. Pai, C.-F., Mann, M., Tan, A. J. & Beach, G. S. D. Determination of spin torque efficiencies in heterostructures with perpendicular magnetic anisotropy. *Phys. Rev. B* **93,** 144409 (2016).

28. Han, D. S. *et al.* Asymmetric hysteresis for probing Dzyaloshinskii-Moriya interaction. *Nano Lett.* **16,** 4438–4446 (2016).

29. Koplak, O. *et al.* Magnetization switching diagram of a perpendicular synthetic ferrimagnet CoFeB/Ta/CoFeB bilayer. *J. Magn. Magn. Mater.* **433,** 91–97 (2017).

30. Yu, G. *et al.* Switching of perpendicular magnetization by spin–orbit torques in the absence of external magnetic fields. *Nat. Nanotechnol.* **9,** 548 (2014).

31. See http://www.flapw.de.

32. Perdew, J. P., Burke, K. & Ernzerhof, M. Generalized Gradient Approximation Made Simple. *Phys. Rev. Lett.* **77,** 3865–3868 (1996).

33. Schweflinghaus, B., Zimmermann, B., Heide, M., Bihlmayer, G. & Blügel, S. Role of Dzyaloshinskii-Moriya interaction for magnetism in transition-metal chains at Pt step edges. *Phys. Rev. B* **94,** 24403 (2016).

Figures

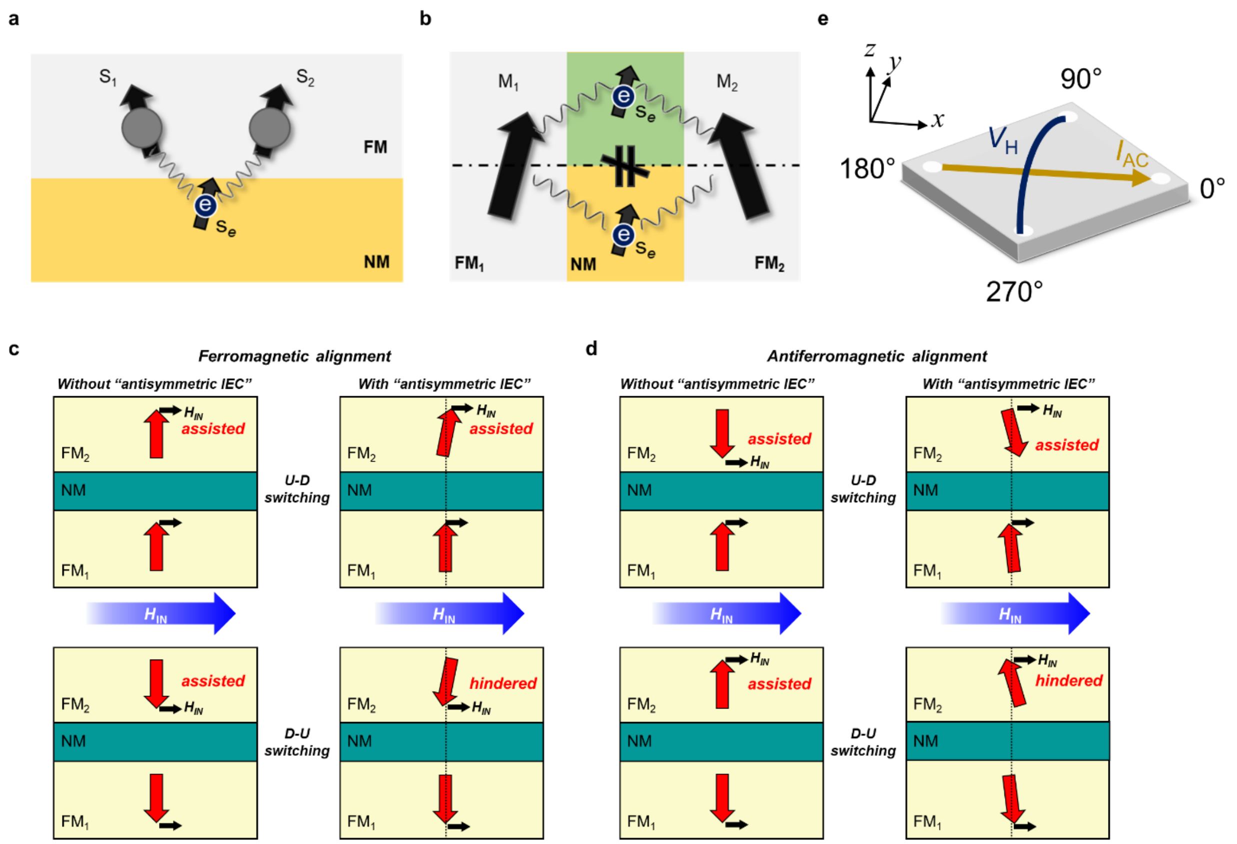

Figure 1| Schematic illustration of antisymmetric exchange coupling and asymmetric switching behavior of perpendicularly magnetized SAFs with parallel and antiparallel coupling by antisymmetric interlayer exchange coupling. Schematic illustration of conduction electron-mediated inter-atomic exchange coupling between two atomic spins (**a**) and magnetic layers (**b**), which give rise to symmetric and antisymmetric inter-atomic and interlayer exchange couplings, respectively. The black arrows in ferromagnets (FMs) represent either localized atomic spins ($S_{1,2}$) or magnetizations ($M_{1,2}$). The gray arrows are spins of conduction electrons in non-magnetic layers (NM). The green and yellow boxes in (**b**) represent a broken inversion symmetry in the plane of films. All non-magnetic layers are assumed to include heavy elements with SOC. Schematics of symmetric and asymmetric switching of perpendicularly magnetized SAFs with parallel (**c**) and antiparallel alignment (**d**) of the layers due to symmetric IEC and additionally in the presence and absence of antisymmetric interlayer coupling, respectively. The chirality of all magnetization configurations displayed for "with antisymmetric IEC" is right-handed. The red arrows indicate magnetizations of top and bottom FMs. The blue arrows represent an in-plane bias field. The in-plane bias field (H_{IN}) breaks the inversion symmetry between up-to-down (U-D) and down-to-up (D-U) switching polarities only in the presence of antisymmetric interlayer coupling, due to the chiral magnetization alignments. **e** Schematics of the experiments. The AHE is measured in the full sheet samples by using a Van der Pauw method. The ac current is applied parallel to the *x*-axis that is along the 0°-180° line.

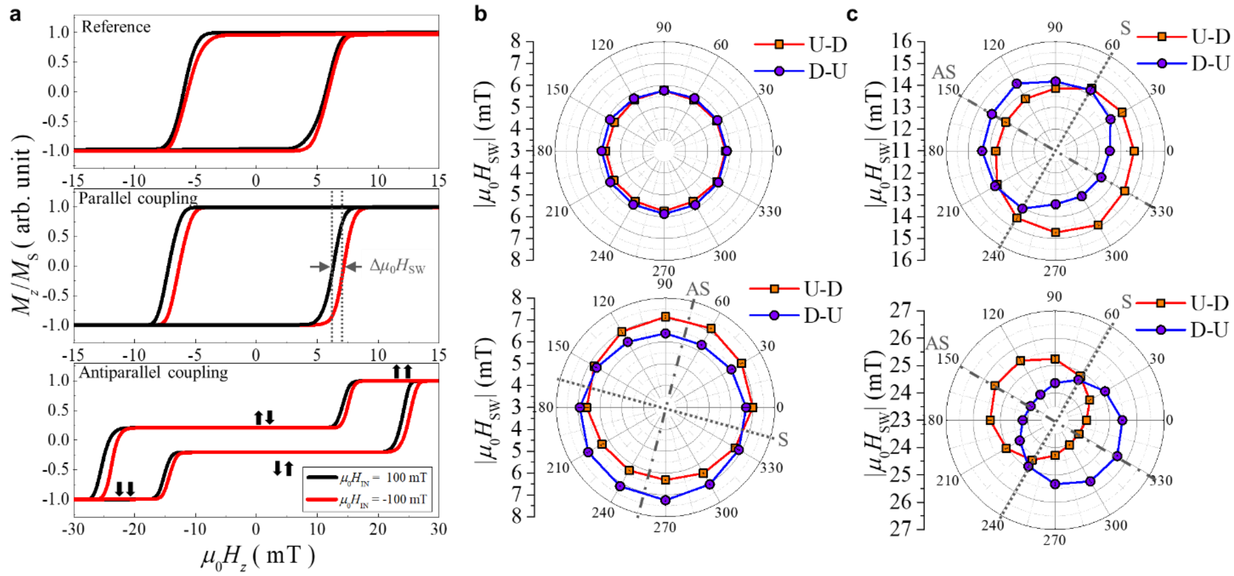

Figure 2 Chiral and unidirectional magnetization switching behaviors. a Magnetic hysteresis loops measured by anomalous Hall effect for the reference Pt/Co/Pt/Ru (top panel) and SAFs of Pt/Co/Pt/Ru/Pt/Co/Pt with parallel (middle panel) and antiparallel (bottom panel) coupling. The black and red curves indicate the hysteresis loops under the application of the negative and positive in-plane field of $|\mu_0 H_{IN}|$ = 100mT, respectively, which applied along **AS** axis, as indicated in Fig. 2b and 2c. For the Pt/Co/Pt/Ru/Pt/Co/Pt, the difference in switching fields, $\Delta\mu_0 H_{SW}$ between U-D and D-U corresponds to ~0.7mT. Four representative magnetization configurations which appear during magnetization reversal are indicated as black arrows. **b** Azimuthal-angular dependence of switching field of Pt/Co/Pt/Ru (top panel) and ferromagnetically coupled multilayers of Pt/Co/Pt/Ru/Pt/Co/Pt (bottom panel). The red and blue symbols are for U-D and D-U switching polarities, respectively. The lines are to guide the eyes. **c** Azimuthal-angular dependence of switching field of top (top panel) and bottom (bottom panel) Co layers of antiferromagnetically coupled Pt/Co/Pt/Ru/Pt/Co/Pt. **AS** and **S** represent asymmetric and symmetric axes, respectively.

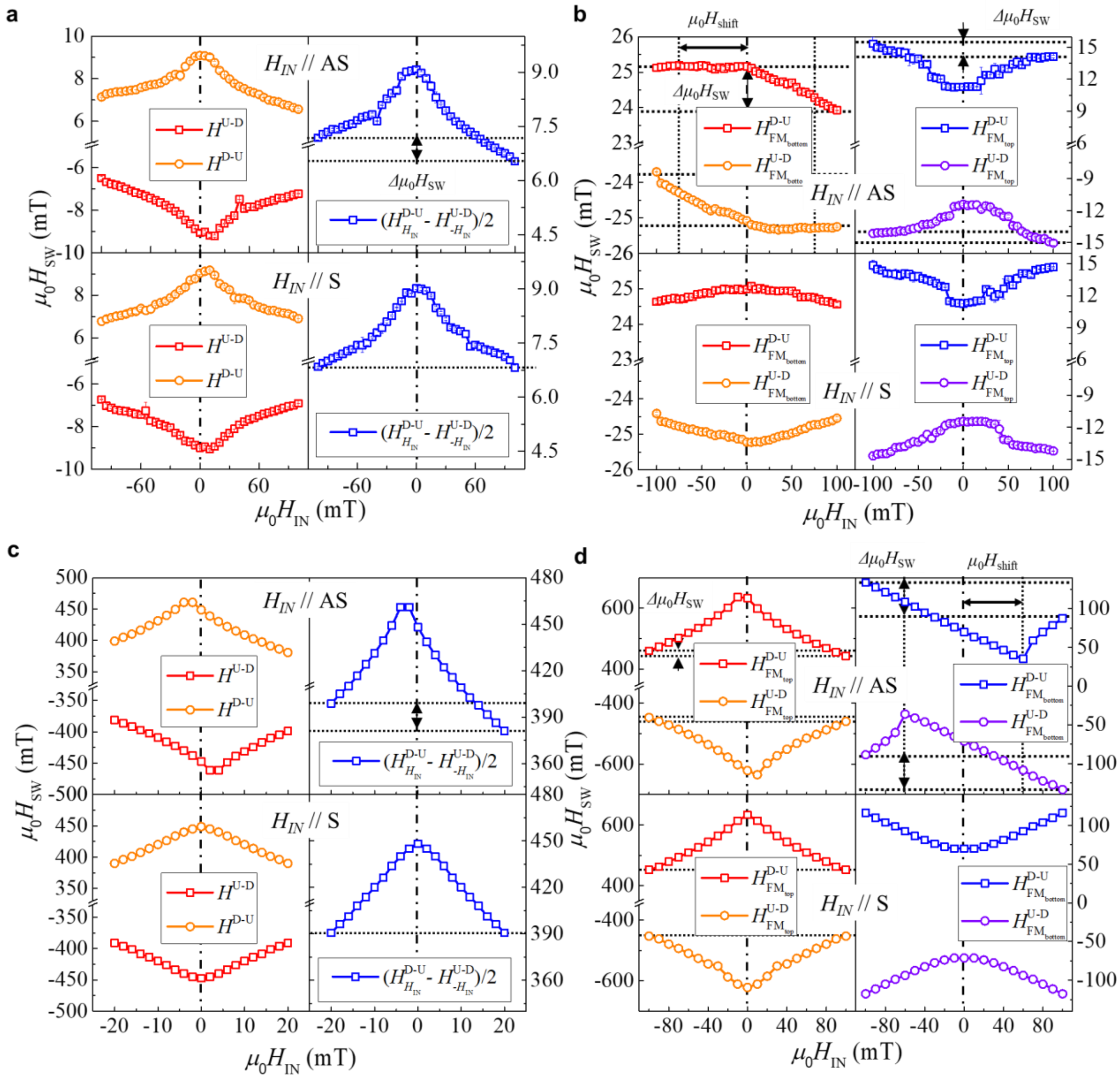

Figure 3 In-plane field dependence of magnetization switching fields. Experimentally measured switching field H_{SW} as a function of H_{IN}, applied along **AS** (top panel) and **S** (bottom panel) axes as defined in Fig. 2, in SAFs with parallel (**a**) and antiparallel (**b**) coupling. The right panels on each column of (**a**) represent averaged $|H_{SW}|$ of U-D and D-U switching for H_{IN} and **-**H_{IN}, respectively. For both parallel and antiparallel coupled cases, the symmetric (asymmetric) H_{SW} with respect to H_{IN}=0 is found when H_{IN} is applied along **S** (**AS**) axis. Calculated H_{SW} as a function of H_{IN} for SAFs with parallel (**c**) and antiparallel (**d**) coupling by using a macro spin model (Methods section).

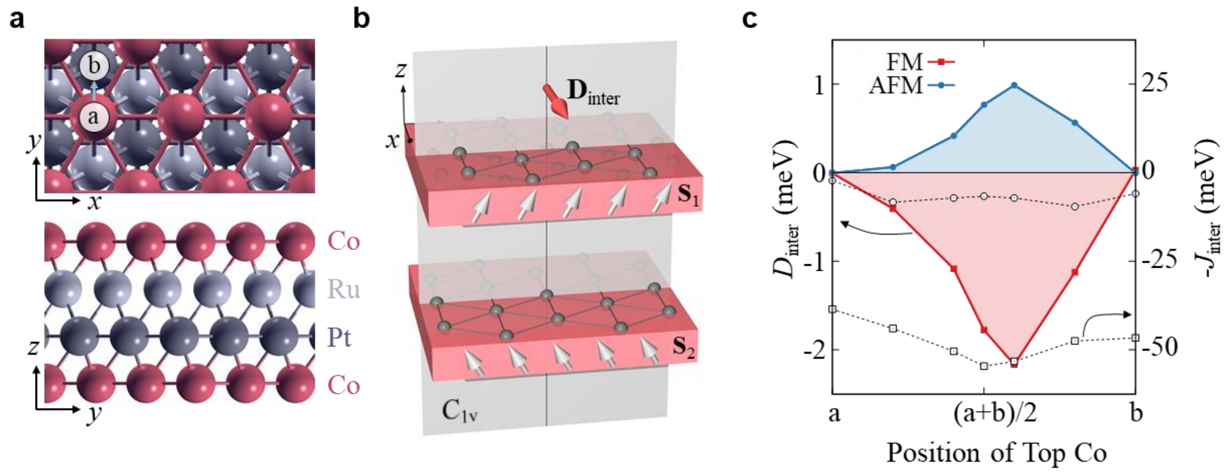

Figure 4 Antisymmetric interlayer exchange from first principles. (**a**) Top and side view of the thin Co/Ru/Pt/Co film. The high-symmetry locations "a" and "b" are marked, and the colored arrow indicates the direction of the considered displacements of the top Co layer. (**b**) Microscopic schematic of the chiral interlayer exchange in the C_{1v} structures. The collinear magnetization (grey arrows) of adjacent magnetic layers acquires a relative canting due to the antisymmetric interlayer interaction as mediated by $\boldsymbol{D}_{\text{inter}}$, which is perpendicular to the shaded mirror plane. (**c**) Effective interlayer coupling constants D_{inter} (solid lines) and $-J_{\text{inter}}$ (dotted lines) as a function of the position of the top Co layer, where squares and circles refer to the cases of parallel and antiparallel coupling, respectively.